Molecular Microbiology (2008) 70(3), 634–651 ■
doi:10.1111/j.1365-2958.2008.06432.x
First published online 24 September 2008

Localization of PBP3 in *Caulobacter crescentus* is highly dynamic and largely relies on its functional transpeptidase domain

Teresa Costa,[1†] Richa Priyadarshini[1] and Christine Jacobs-Wagner[1,2*]
[1]*Department of Molecular, Cellular, and Developmental Biology, Yale University, New Haven, CT 06520, USA.*
[2]*Howard Hughes Medical Institute, New Haven, CT 06520, USA.*

Summary

In rod-shaped bacteria, septal peptidoglycan synthesis involves the late recruitment of the *ftsI* gene product (PBP3 in *Escherichia coli*) to the FtsZ ring. We show that in *Caulobacter crescentus*, PBP3 accumulates at the new pole at the beginning of the cell cycle. Fluorescence recovery after photobleaching experiments reveal that polar PBP3 molecules are, constantly and independently of FtsZ, replaced by those present in the cellular pool, implying that polar PBP3 is not a remnant of the previous division. By the time cell constriction is initiated, all PBP3 polar accumulation has disappeared in favour of an FtsZ-dependent localization near midcell, consistent with PBP3 function in cell division. Kymograph analysis of time-lapse experiments shows that the recruitment of PBP3 to the FtsZ ring is progressive and initiated very early on, shortly after FtsZ ring formation and well before cell constriction starts. Accumulation of PBP3 near midcell is also highly dynamic with a rapid exchange of PBP3 molecules between midcell and cellular pools. Localization of PBP3 at both midcell and pole appears multifactorial, primarily requiring the catalytic site of PBP3. Collectively, our results suggest a role for PBP3 in pole morphogenesis and provide new insights into the process of peptidoglycan assembly during division.

Accepted 25 August, 2008. *For correspondence. E-mail christine.jacobs-wagner@yale.edu; Tel. (+1) 203 432 5170; Fax (+1) 203 432 6161. †Present address: Instituto de Tecnologia Química e Biológica, Universidade Nova de Lisboa, 2780-157 Oeiras, Portugal.

© 2008 The Authors
Journal compilation © 2008 Blackwell Publishing Ltd

Introduction

Growth and division of bacterial cells require the enlargement of their complex cell wall (Nanninga, 1991; 1998; Höltje, 1998; Koch, 2000). The major component of the cell wall is the peptidoglycan (PG), a polymer of cross-linked glycan strands that forms a strong and elastic exoskeleton essential for maintaining cell shape and withstanding intracellular pressure (Höltje, 1998; Nanninga, 1998; Cabeen and Jacobs-Wagner, 2005; Vollmer *et al.*, 2008). The glycan strands of PG are composed of an alternating disaccharide subunit of *N*-acetylglucosamine and *N*-acetylmuramic acid covalently linked to a peptide. Linear glycan chains are cross-linked through peptide cross-bridges by transpeptidation, forming the characteristic PG structural mesh-like layer. PG synthesis occurs through the concerted action of synthases and hydrolases present in complexes (Romeis and Höltje, 1994; von Rechenberg *et al.*, 1996; Vollmer *et al.*, 1999), presumably to provide safe cell wall enlargement during growth and division (Höltje, 1996; 1998). Cell division and septal PG synthesis lead to the formation of new cell poles where PG synthesis shuts down (Woldringh *et al.*, 1987; de Pedro *et al.*, 1997), although recent evidence suggests that there is residual PG metabolic activity during a short period following division (Rafelski and Theriot, 2006; Tiyanont *et al.*, 2006; Aaron *et al.*, 2007).

Synthesis of septal PG depends on the assembly of the cytoskeletal tubulin homologue FtsZ at the future site of division (Errington *et al.*, 2003; Lutkenhaus, 2007). FtsZ assembly occurs before cytokinesis is initiated, and the FtsZ ring contributes to pre-septal cell elongation by recruiting MurG, an enzyme involved in the synthesis of the PG precursor Lipid II, a key intermediate in PG biosynthesis (de Pedro *et al.*, 1997; van Heijenoort, 1998; Rothfield, 2003; Aaron *et al.*, 2007; Mohammadi *et al.*, 2007). The contribution of FtsZ to cell elongation can be considerable in bacteria like *Caulobacter crescentus* where there is a large temporal gap between FtsZ ring formation and the initiation of cell constriction (Aaron *et al.*, 2007). Later, FtsZ mediates cell division by providing a scaffold for the sequential recruitment of other cell division proteins (to form the so-called divisome)

(Errington *et al*., 2003; Goehring *et al*., 2006). In *Escherichia coli*, the mature divisome includes FtsZ, ZipA/FtsA/ZapA, FtsE/X, FtsK, FtsQ, FtsB/L, FtsW, PBP3, FtsN, AmiC and EnvC (Goehring and Beckwith, 2005; den Blaauwen *et al*., 2008). Each protein requires upstream proteins to localize, reflecting a temporal sequence of recruitment. A current model proposes that the assembly and maturation of the divisome occurs in two defined steps (Aarsman *et al*., 2005). First, FtsZ assembles into a ring and recruits early-division proteins (such as ZipA, ZapA and FtsA); this step promotes a switch in the predominant mode of PG synthesis from cylindrical to medial, which contributes to pre-septal elongation. In the second step, which occurs after a certain delay, late cell division proteins assemble at the FtsZ ring to form the mature divisome, right around the onset of cell constriction.

PBP3, which is encoded by the *ftsI* gene, is one of the late-division proteins (Weiss *et al*., 1997; Wang *et al*., 1998). It is a membrane-bound class B high-molecular-weight (HMW) PBP that contains a short cytoplasmic region, a single transmembrane (TM) sequence, and a periplasmic domain of unknown function followed by a C-terminal transpeptidase domain involved in PG cross-linking (Kraus and Höltje, 1987; Bowler and Spratt, 1989; Nguyen-Distèche *et al*., 1998). PBP3 interacts with class A PBP1B, the monofunctional glycosyltransferase (MtgA) and a lytic transglycosylase to form a multienzyme complex that mediates incorporation and cross-linking of glycan strands co-ordinately (Romeis and Höltje, 1994; Bertsche *et al*., 2006; Derouaux *et al*., 2008). Depletion or chemical inactivation of PBP3 inhibits cell division, resulting in cell filamentation (Spratt, 1977; Curtis *et al*., 1985; Yanouri *et al*., 1993; Ohta *et al*., 1997). In *E. coli*, PBP3 appears to be recruited to the divisome largely through interactions with several proteins of the divisome complex (Di Lallo *et al*., 2003; Corbin *et al*., 2004; Karimova *et al*., 2005). For instance, FtsW is required for PBP3 localization to the division site (Mercer and Weiss, 2002), presumably via an interaction with a short N-terminal region of PBP3 that includes the membrane anchor (Piette *et al*., 2004; Karimova *et al*., 2005). The TM segment alone is sufficient to mediate the accumulation of GFP at midcell, although to a lesser degree than the full-length protein (Wissel *et al*., 2005).

Here we examine the temporal and spatial distribution of PBP3 in the Gram-negative bacterium *C. crescentus*. The ease of obtaining cell cycle-synchronized populations and the large delay between FtsZ ring formation and cell constriction make this bacterium a valuable model for such study. The *C. crescentus* cell cycle starts with the 'swarmer' cell, which carries a flagellum at the 'old' pole (i.e. pole opposite to the 'new' pole formed by the last division). The swarmer cell elongates through patchy or seemingly helical insertion of PG synthesis along the lateral walls (Aaron *et al*., 2007; Divakaruni *et al*., 2007). This is followed by the assembly of the FtsZ ring and redistribution of most PG synthesis at the site of the FtsZ ring (Kelly *et al*., 1998; Aaron *et al*., 2007). At this stage, a stalk (a thin extension of the cell envelope involved in nutrient uptake and cell attachment) forms at the old pole after flagellum ejection. Elongation of the stalked cell produces a pre-divisional cell, which builds a flagellum at the new pole. Cell division generates a swarmer daughter cell (which repeats the sequence described above) and a stalked daughter cell, which skips the swarmer cell stage and immediately assembles the FtsZ ring. By simultaneously visualizing PBP3 and FtsZ fusions to fluorescent proteins by time-lapse microscopy, we establish the precise temporal sequence of PBP3 and FtsZ distribution during the cell cycle. While there is a notable delay between FtsZ ring formation and PBP3 assembly at the divisome, the recruitment of PBP3 to the FtsZ ring is initiated well before the onset of cell constriction and occurs very gradually. After division, PBP3 localizes at the new pole in a dynamic and FtsZ-independent manner. We also found that the transpeptidase catalytic site of PBP3 is important for both polar and divisomal localization of PBP3. These findings provide new insights into the processes of divisome assembly and PG synthesis.

Results

The essential cell division protein PBP3 changes its spatial distribution during the cell cycle

Consistent with a conserved function for PBP3 in cell division, Ohta *et al*. (1997) showed that *C. crescentus* CB15 cells carrying an uncharacterized temperature-sensitive (Ts) mutation in the *ftsI* gene [*ftsI*(Ts), therein referred to as *divA305*] formed long cell filaments when grown at the restrictive temperature. We transferred this *ftsI*(Ts) mutation (linked to a gentamicin resistance cassette) to the synchronizable CB15N background (creating strain CJW2141) where the Ts cell division phenotype was recapitulated (Fig. 1A). Sequencing the *ftsI*(Ts) allele revealed a mutation (A808T) that causes an amino acid substitution (Y270N) of a highly conserved residue within the transpeptidase domain of PBP3 (Goffin and Ghuysen, 1998).

In *E. coli*, polymerization of FtsZ at midcell is a prerequisite step for the recruitment of PBP3 to the divisome complex (Wang *et al*., 1998; Weiss *et al*., 1999). While FtsZ localization contributes both to pre-septal elongation and cell division, PBP3 is thought to act exclusively during cell division. Consistent with this idea, *E. coli* PBP3 localizes after FtsZ ring formation at a time corresponding approximately to the initiation of cell constriction. This is inferred from the observation that PBP3 localizes at

© 2008 The Authors
Journal compilation © 2008 Blackwell Publishing Ltd,

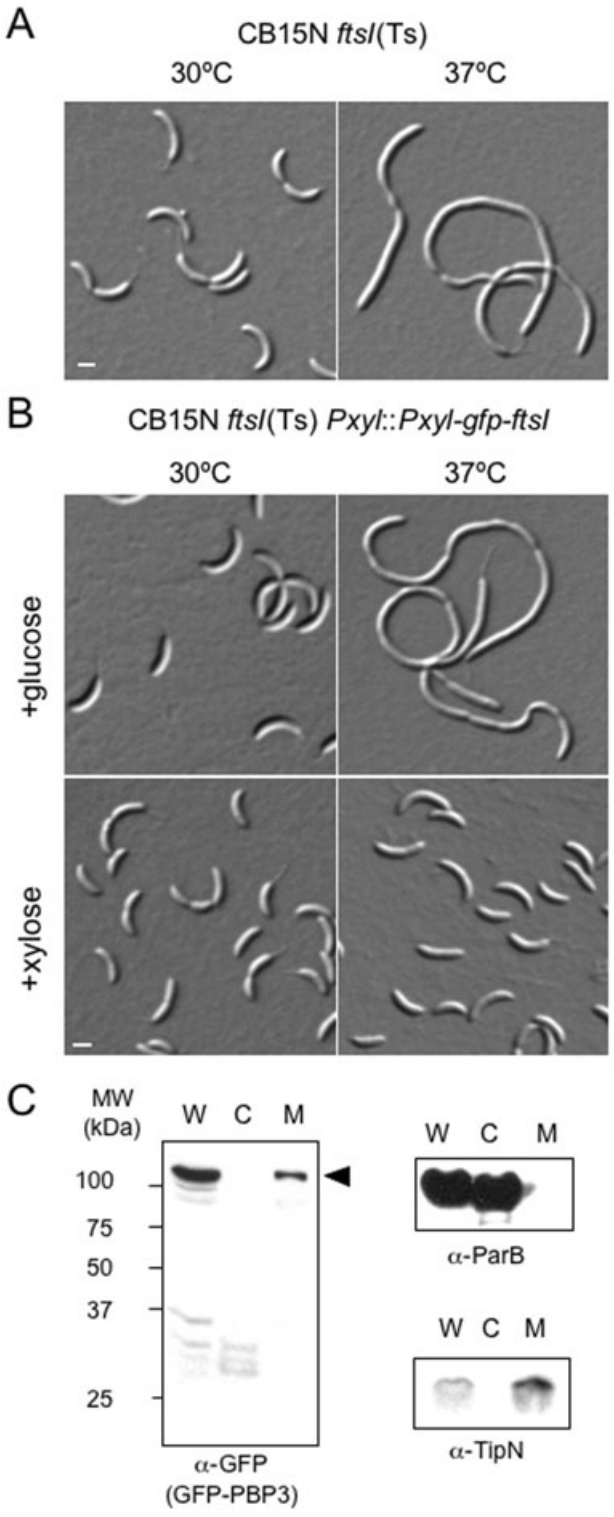

Fig. 1. GFP–PBP3 suppresses the cell division defect of an *ftsI*(Ts) mutation.
A. Differential interference contrast (DIC) images of *ftsI*(Ts) mutant cells (CJW2141) grown at 30°C then used to inoculate fresh medium that was then incubated at either 30°C or 37°C for 3 h. The cultures were kept in log-phase.
B. The *ftsI*(Ts) filamentous phenotype was complemented by expression of a *gfp–ftsI* allele under control of *Pxyl* when cells [CJW2235, CB15N *ftsI*(Ts) P*xyl*::*Pxyl–gfp–ftsI*] were grown for 3 h at 37°C in the presence of xylose (inducer), but not in the presence of 0.2% glucose.
Scale bar, 1 μm.
C. Immunoblot blot analysis of samples obtained from biochemical fractionation using anti-GFP, anti-TipN and anti-ParB antibodies. Whole-cell samples were prepared by sonication of CJW1822 cells (CB15N *Pxyl*::*Pxyl–gfp–ftsI*) grown in the presence of xylose (to produce GFP–PBP3). W, whole-cell extract; M, membrane fraction; C, cytoplasmic fraction; MW, molecular weight markers.

midcell in only about 50% of exponential-phase *E. coli* cells (Weiss *et al*., 1999) whereas 90% of cells in similar growth phase display midcell FtsZ localization (Ma *et al*., 1996). Moreover, independent fluorescence microscopy experiments using the appearance of cell constriction as a temporal landmark suggest a delay of 14–21 min between FtsZ ring formation and midcell recruitment of PBP3 (Den Blaauwen *et al*., 1999; Aarsman *et al*., 2005). To gain temporal resolution, we wanted to visualize FtsZ and PBP3 simultaneously while the cells proceeded through the cell cycle. We reasoned that the large time gap between FtsZ assembly and cell constriction in *C. crescentus* (Kelly *et al*., 1998) should help in visualizing any temporal differences that may exist among FtsZ assembly, PBP3 localization and cell constriction. We therefore integrated a *gfp–ftsI* fusion under the control of the xylose-dependent promoter (*Pxyl*) at the *xylX* chromosomal locus in a strain carrying *ftsZ–mcherry* under the vanillate-inducible promoter (*Pvan*) at the *vanA* locus (creating strain CJW1823, which also carries *ftsI* and *ftsZ* at their native loci). The functionality of GFP–PBP3 was inferred from its ability to rescue the Ts cell division defect of *ftsI*(Ts) cells (strain CJW2235) in a xylose-dependent fashion (Fig. 1B). Immunoblot analysis showed that the full-length GFP–PBP3 fusion [together with a minor C-terminal truncated form that may correspond to C-terminal processing (Nakamura *et al*., 1983; Hara *et al*., 1989; Nagasawa *et al*., 1989)] accumulated under xylose induction but not when synthesis was blocked by substitution of xylose by glucose (Fig. S1). Biochemical fractionation followed by immunoblotting (Fig. 1C) confirmed that GFP–PBP3 was membrane-bound. The TM protein TipN and the cytoplasmic protein ParB were used to verify the quality of the fractionation.

Time-course experiments of synchronized CJW1823 cell populations (CB15N *Pxyl*::*Pxyl–gfp–ftsI Pvan*::*Pvan–ftsZ–mcherry*) producing both GFP–PBP3 and FtsZ–mCherry revealed that the GFP–PBP3 signal, in addition to a cellular distribution, accumulated at the new pole (i.e. previous site of division) of swarmer cells (Fig. 2A), just as FtsZ (Thanbichler and Shapiro, 2006). The polar accumulation of GFP–PBP3 was unlikely to be due to an overproduction effect, as this fusion protein also localized at the

© 2008 The Authors

pole in cells (CJW2144; CB15N *ftsI*::*gfp–ftsI*) expressing *gfp–ftsI* as a single copy under the control of the *ftsI* native promoter (Fig. 3A). While FtsZ–mCherry moved from the new pole to form a band (ring) near midcell early in the cell cycle as previously reported (Kelly *et al*., 1998; Thanbichler and Shapiro, 2006), the polar GFP–PBP3 focus remained apparent for a longer period of time (Fig. 2A). By the time cell constriction was visible, the polar GFP–PBP3 focus had disappeared and GFP–PBP3 displayed a strong band-like localization at the FtsZ–mCherry ring location (Fig. 2A). The FtsZ–mCherry and GFP–PBP3 colocalization persisted throughout cell constriction, consistent with the role of PBP3 in cell division. Division yielded daughter cells with a PBP3 focus at the new pole. It should be noted that all cells, irrespective of their cell cycle stage, also displayed a diffuse cellular fluorescent signal (Fig. 2A). This signal (which was above background, data not shown) largely corresponded to GFP–PBP3 proteins diffusively distributed around the membrane based on biochemical fractionation (Fig. 1C). In *C. crescentus*, membranal localization of TM proteins produced in low abundance is often not evident by epifluorescence microscopy (Wheeler and Shapiro, 1999; Obuchowski and Jacobs-Wagner, 2008). This is because *C. crescentus* cells are quite thin (about 0.5 μm of width) relative to other model bacteria such as *E. coli* or *Bacillus subtilis*.

To determine the relative localization of PBP3 and FtsZ with greater temporal resolution, we acquired short time-interval sequences of FtsZ–mCherry and GFP–PBP3 localization during the cell cycle, starting with swarmer cells. Kymographs of these time-lapse recordings were constructed to display the maximum pixel intensity of FtsZ–mCherry and GFP–PBP3 fluorescence distribution along the cell length as a function of time (Fig. 2B; the kymographs were inverted to facilitate visualization of the fluorescence signal). They showed that both FtsZ–mCherry and GFP–PBP3 accumulate at the new pole during the swarmer cell stage. During the swarmer-to-stalked cell transition, FtsZ–mCherry signal moves from the pole and then exhibits a period of high mobility within the medial cell region before stabilizing at one position (Fig. 2B), in agreement with a previous report (Thanbichler and Shapiro, 2006). Surprisingly, kymograph analysis consistently showed that during a certain period of time (shown in light orange in Fig. 2B), the GFP–PBP3 signal is split between a medial localization and a polar accumulation. This split starts at 0.25 ± 0.07 cell cycle units ($n = 17$) shortly after FtsZ–mCherry stabilizes at one position at 0.15 ± 0.06 cell cycle units ($n = 17$). Over time, the medial GFP–PBP3 signal progressively increases at the expense of the polar signal. By the time cell constriction initiates (0.51 ± 0.10 cell cycle units, $n = 17$), all polar signal has disappeared and GFP–PBP3 exhibits a strong medial signal. (Note that the fluorescence signal corresponding to the GFP–PBP3 cellular pool was subtracted in the kymograph shown in Fig. 2B for better visualization of the overlapping period between polar and medial localization of GFP–PBP3.) The time overlap between polar and medial localization was also observed when GFP–PBP3 was expressed at endogenous levels under native conditions (Fig. 3B). Thus, a fraction of PBP3 molecules is recruited to the FtsZ ring in the elongation phase shortly after FtsZ assembly and well before cell constriction becomes visible. Accumulation of PBP3 at the FtsZ ring is clearly progressive and apparently at the expense of its polar localization.

FtsZ is required for the localization of PBP3 to the division site, but not for its maintenance at the pole

Next, we investigated the dependency of PBP3 localization on FtsZ. For this, we generated a strain (CJW2143, CB15N *ftsI*::*gfp–ftsI ftsZ*::*Pxyl–ftsZ*) that carries a *gfp–ftsI* fusion under native expression (as the only *ftsI* copy) and *ftsZ* under xylose-dependent expression to visualize GFP–PBP3 under conditions of FtsZ depletion. After growth in xylose-containing medium, swarmer cells of CJW2143 were obtained and re-suspended in liquid medium containing either xylose to maintain FtsZ synthesis or glucose to initiate immediate FtsZ depletion (Wang *et al*., 2001). Under FtsZ-depletion conditions (glucose), GFP–PBP3 failed to accumulate near midcell (Fig. 4A; representative time points are shown). Instead, GFP–PBP3 retained a polar localization for extended periods of time in the elongating FtsZ-depleted cells. Quantitative analysis (Fig. 4B) showed that the percentage of cells with a polar GFP–PBP3 focus remained relatively steady over time in the absence of FtsZ (glucose). Under condition of FtsZ synthesis (xylose), the cells exhibited a normal cell cycle profile of PBP3 localization with the polar accumulation being progressively replaced by a medial localization (Fig. 4C). The reappearance of polar GFP–PBP3 in some FtsZ-producing cells at the last time points (80 min; Fig. 4C) corresponded to cells that had divided (data not shown). These results show that FtsZ is required for PBP3 recruitment to the future division site, as expected. They also confirm that the medial localization of PBP3 comes at the expense of polar localization as polar localization persists when medial localization is prevented, consistent with a competitive relationship between the two localization sites.

PBP3 is dynamically recruited to the pole in an FtsZ-independent manner

A trivial explanation for the polar localization of PBP3 is that it corresponds to a remnant of PBP3 molecules from the previous divisome. If that were the case, polar PBP3

© 2008 The Authors

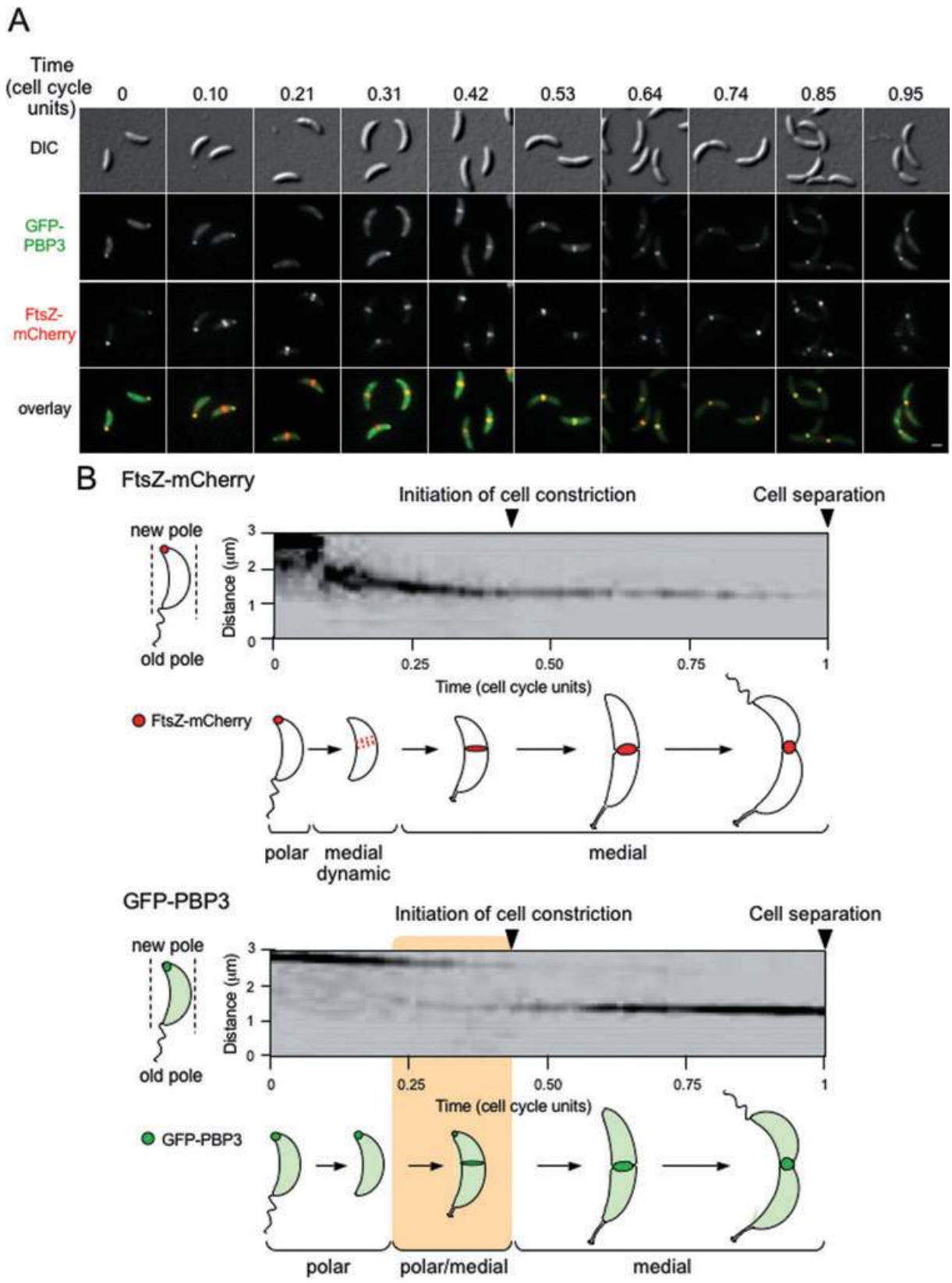

© 2008 The Authors

Fig. 2. Recruitment of PBP3 to the FtsZ ring is gradual and occurs well before cell constriction begins.
A. CJW1823 cells (CB15N *Pxyl*::*Pxyl–gfp–ftsI Pvan*::*Pvan–ftsZ–mcherry*) producing GFP–PBP3 and FtsZ–mCherry were cultured for 6 h in xylose and 2 h in vanillic acid. After synchronization, swarmer cells were grown in fresh media containing xylose and vanillic acid. Samples were collected immediately upon synchronization and at 10 min intervals thereafter, and examined by DIC and fluorescence microscopy. Under these time-course conditions, the cell cycle takes about 100 min; the time is indicated in cell cycle units. Scale bar, 1 μm.
B. Inverted kymographs of a time-lapse sequence of FtsZ–mCherry and GFP–PBP3 signals in a single cell during the course of its cell cycle. Production of FtsZ–mCherry and GFP–PBP3 was induced by growing CJW1823 cells for 2 and 6 h in vanillic acid and xylose respectively. The cells were then placed on an agarose-padded slide containing xylose and vanillic acid, and FtsZ–mCherry and GFP–PBP3 localization was examined every 2 min for about 224 min, which, under these growth conditions, approximately corresponded to the cell cycle length (time is indicated in cell cycle units). Kymographs display the maximum intensity values of FtsZ–mCherry and GFP–PBP3 signals along the long axis of the cell for each frame, using a 3-μm-wide region (dotted lines). The cell is oriented such that its new and old poles are at the top and bottom of each kymograph panel respectively. The times corresponding to the initiation of cell constriction and to cell separation are indicated.

molecules would be stationary, and photobleaching the polar focus of GFP–PBP3 should lead to no fluorescence recovery, as there would be no exchange between polar GFP–PBP3 and the diffuse membranal pool of PBP3. However, fluorescence recovery after photobleaching (FRAP) experiments in CJW1823 cells (CB15N *Pxyl*::*Pxyl–gfp–ftsI Pvan*::*Pvan–ftsZ–mcherry*) showed that the bleached polar GFP–PBP3 signal recovered very rapidly with an average half-time of 25 ± 9 s ($n = 38$ cells) (Fig. 5A). We selectively bleached cells in which FtsZ–mCherry was no longer polar to show that fluorescence recovery occurred independently of FtsZ (Fig. 5A). Consistent with rapid exchange of GFP–PBP3 molecules between polar and membrane pools, the fluorescence intensity of unbleached cellular regions (after normalization to account for photobleaching from image acquisition) decreased concomitantly with the fluorescence recovery in the bleached polar region (Fig. 5A). We also observed rapid signal recovery at the pole after photobleaching in cells that did not produce an FtsZ–mCherry fusion (Fig. S2A; half-time = 19 ± 7 s, $n = 83$ cells) or that were treated with chloramphenicol (CAM) to block protein synthesis (Fig. S2B; 28 ± 6 s, $n = 38$ cells). This demonstrates that the fast fluorescence recovery was largely due to an exchange between polar and membranal pools, and not because of *de novo* synthesis of GFP–PBP3. It was not artificially caused by the overproduction of GFP–PBP3 or the presence of untagged PBP3 because we

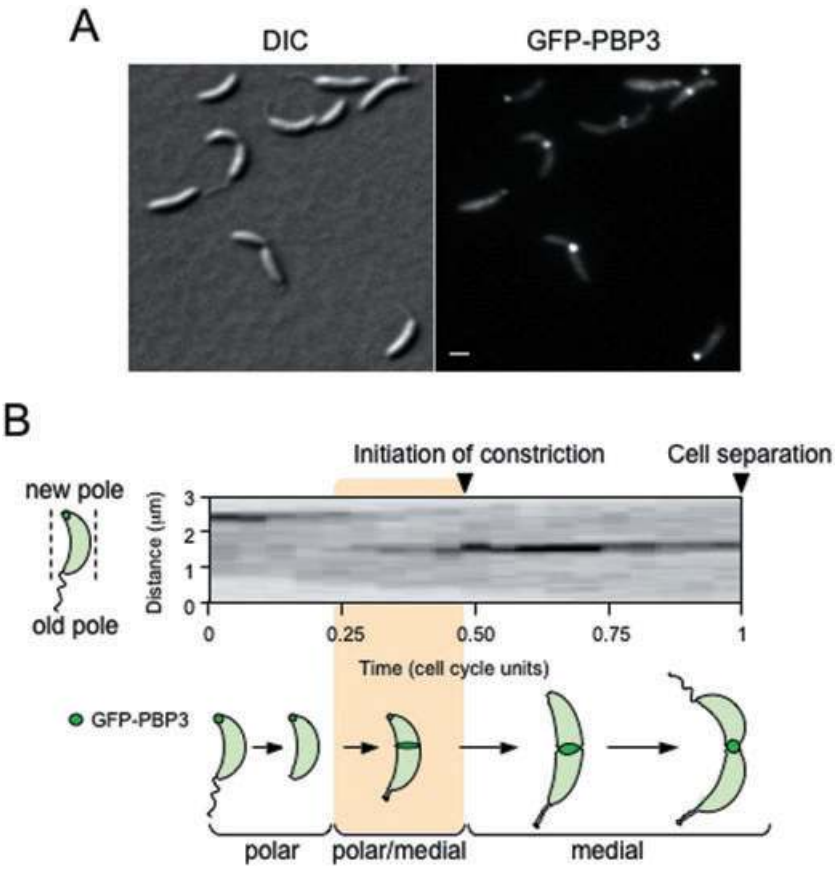

Fig. 3. GFP–PBP3 produced from the *ftsI* promoter as the only source of PBP3 displays a similar pattern of localization to GFP–PBP3 produced from *Pxyl*.
A. Fluorescence microscopy and DIC images of an asynchronous population of CJW2144 (CB15N *ftsI*::*gfp–ftsI*) cells in which wild-type *ftsI* has been replaced by a *gfp–ftsI* fusion. GFP–PBP3 was found at the pole or at a medial position in 75% of non-constricted cells ($n = 65$) and 84% of constricted cells ($n = 64$) respectively. Scale bar, 1 μm.
B. Representative inverted kymograph of time-lapse microscopy sequences of CJW2144 cells. Kymographs were constructed as described in Fig. 2B except that images were acquired every 10 min.

© 2008 The Authors
Journal compilation © 2008 Blackwell Publishing Ltd,

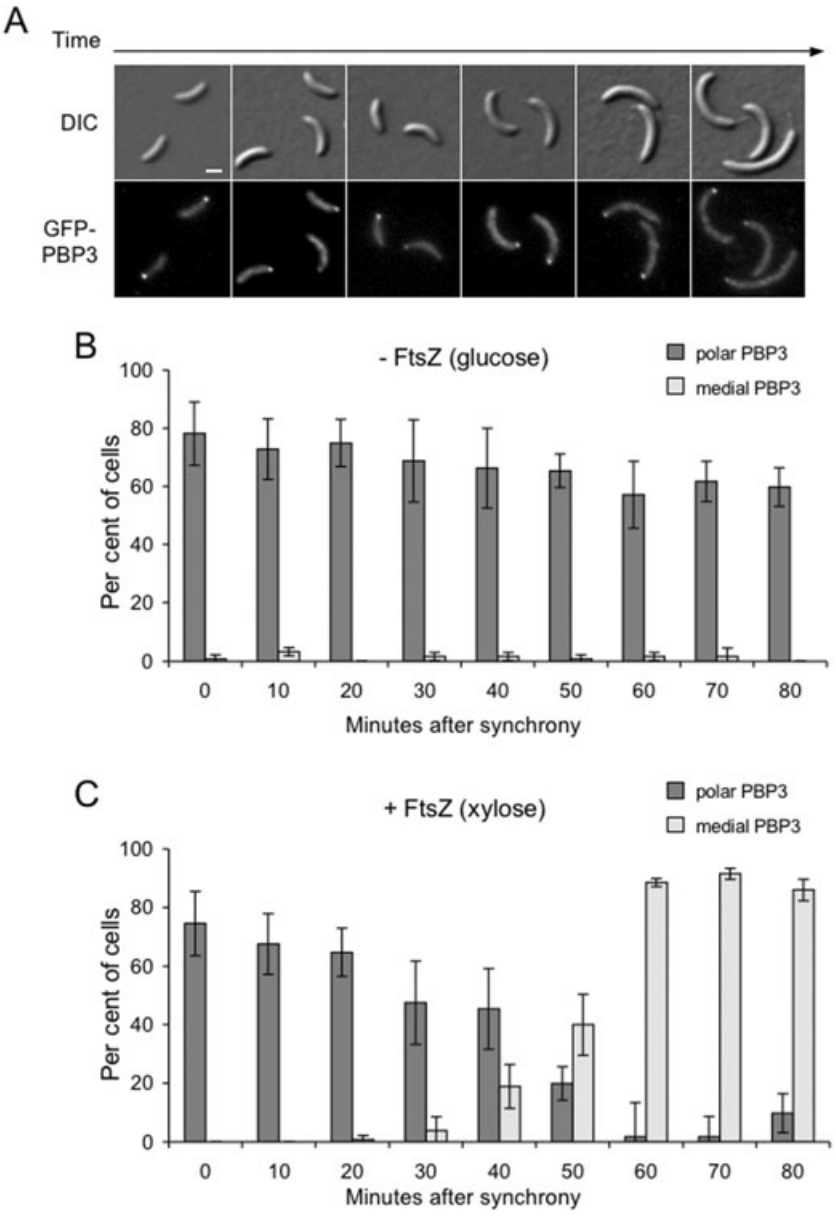

Fig. 4. Polar localization of GFP–PBP3 persists longer when medial localization is prevented by FtsZ depletion. Localization of GFP–PBP3 in FtsZ-depleted cells was examined in time-course experiments starting with CJW2143 swarmer population (CB15N *ftsI*::*gfp–ftsI ftsZ*::*Pxyl*::*ftsZ*). After growth in PYE + xylose and synchronization, CJW2143 swarmer cells were re-suspended in PYE medium containing either xylose (for FtsZ production) or glucose [for immediate FtsZ depletion because FtsZ is degraded in the swarmer cell stage (Wang *et al*., 2001)]. Samples were collected just after synchrony ($t = 0$ min) and every 10 min thereafter. Under these growth conditions (PYE liquid medium, 30°C), division in FtsZ-producing cells occurs about 80 min after synchronization.
A. Representative images of DIC and fluorescence microscopy of FtsZ-depleted cells producing GFP–PBP3. Selected time points (0, 10, 30, 50, 80 and 90 min) after synchrony are shown. GFP–PBP3 retains a polar localization during elongation when FtsZ is depleted. Scale bar, 1 μm.
B. Quantitative analysis of GFP–PBP3 localization in the absence of FtsZ (glucose condition) following synchrony. At least 120 cells from three separate time-course experiments were considered for this analysis.
C. Quantitative analysis of GFP–PBP3 localization when FtsZ is produced (xylose condition) following synchrony.

also obtained short half-time values of polar recovery (11 ± 6 s, $n = 27$ cells) with cells that produced GFP–PBP3 at native levels as the only source of PBP3 (Fig. S2C). Thus, the polar accumulation of PBP3 does not simply correspond to a remnant from the last division. Instead, PBP3 is actively recruited to the pole in a very dynamic manner independently of FtsZ.

GFP–PBP3 is dynamically recruited to the division site

It is often implicitly assumed that mature divisome complexes remain at the constriction site during the whole division process. However, the fact that PBP3 was found to be dynamically recruited to the cell pole led us to investigate whether PBP3 localization at the division complex is also a dynamic process. Similarly to polar PBP3, the medial GFP–PBP3 signal rapidly recovered after photobleaching with an average recovery half-time of 18 ± 5 s ($n = 146$ cells; Fig. 5B). When we measured the fluorescence intensity of unbleached regions, including only the 'swarmer half' or the 'stalked half' of predivisional cells, we observed that regions in both halves decreased similarly in intensity during the course of the FRAP experiment (Fig. 5B), showing no preference. Similar values of fluorescence recovery half-time were obtained in the presence of CAM (12 ± 7 s, $n = 23$

© 2008 The Authors
Journal compilation © 2008 Blackwell Publishing Ltd,

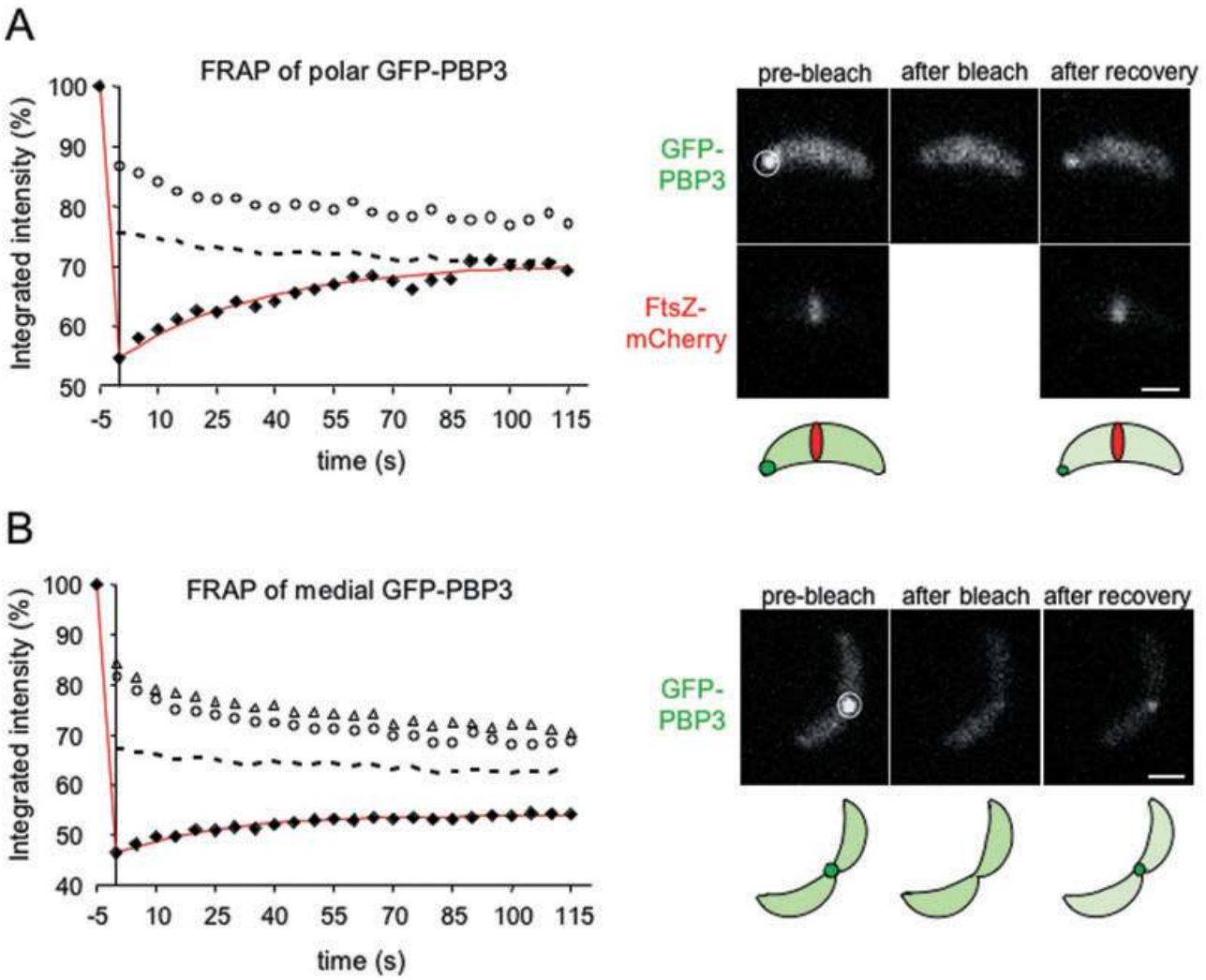

Fig. 5. Both polar and medial GFP–PBP3 molecules are rapidly exchanged with GFP–PBP3 from the cellular (membrane) pool, demonstrating a dynamic process of localization.

A. The exchange of GFP–PBP3 molecules between the polar pool and the rest of the cell was assessed by FRAP analysis. Polar GFP–PBP3 foci of CJW1823 cells (CB15N *Pxyl*::*Pxyl–gfp–ftsI Pvan*::*Pvan–ftsZ–mcherry*) were selectively photobleached in time-lapse sequences in which images were acquired every 5 s before and following photobleaching (the time of photobleaching corresponds to $t = 0$ s). Averaged integrated intensities of the whole cell (dashed line), bleached regions (closed diamonds) and unbleached regions (open circles) were plotted as a function of time. The solid red line is the predicted recovery curve determined by least-squared fitting of the data as described in *Experimental procedures* ($r^2 = 0.95$). The recovery half-time for the bleached polar regions was 25 ± 9 s ($n = 38$ cells). Shown on the right are images of a photobleached cell producing GFP–PBP3 and FtsZ–mCherry before photobleaching (pre-bleach), after bleach and after recovery. The bleached region is indicated by a white circle. The cells selected for photobleaching contained FtsZ–mCherry near midcell before photobleaching and after recovery, demonstrating that the rapid exchange of GFP–PBP3 molecules between polar and cellular pools is not mediated by FtsZ. Scale bar, 1 μm.

B. The exchange of GFP–PBP3 molecules between medial and cellular (membrane) pools was determined by FRAP analysis. GFP–PBP3 signals at the site of division of CJW1822 pre-divisional cells (CB15N *Pxyl*::*Pxyl–gfp–ftsI*) were photobleached as in (A). Integrated intensities were plotted as in (A), except that intensities of unbleached regions from the 'swarmer cell half' (open circles) and 'stalked cell half' (open triangles) of pre-divisional cells are indicated. The recovery half-time for the bleached midcell regions was 18 ± 5 s ($n = 146$ cells). Representative images of a photobleached cell producing GFP–PBP3 are also shown at pre-bleach, after bleach and after recovery. Scale bar, 1 μm.

cells; Fig. S2D) or when *gfp–ftsI* was expressed at native levels as the only *ftsI* copy (16 ± 9 s, $n = 37$; Fig. S2E). Our results demonstrate that GFP–PBP3 molecules at the division site are rapidly exchanged with molecules from the diffuse membranal pool, indicating that no single population of PBP3 molecules continuously participates in septal PG synthesis for long periods of time.

© 2008 The Authors
Journal compilation © 2008 Blackwell Publishing Ltd,

The catalytic site of PBP3 is important for PBP3 localization

In *E. coli*, the N-terminal sequence of PBP3 and in particular its TM segment seem to contain the structural determinants of localization. An N-terminal 56-residue fragment encompassing the cytoplasmic sequence, the TM segment and nine downstream periplasmic residues recapitulates PBP3 septal localization (Piette *et al*., 2004). Point mutations in the PBP3 TM segment or TM sequence swapping with another protein (MalF) disrupt midcell localization (Weiss *et al*., 1999; 2005; Wissel and Weiss, 2004). Furthermore, a short 26-residue sequence containing only the TM segment is sufficient to mediate ring-like localization, albeit not as well as the full-length protein (Wissel *et al*., 2005). Surprisingly, the TM sequence of PBP3 is not well conserved among bacteria, suggesting that either PBP3 targeting sequence varies among species or the TM sequence has co-evolved with its target protein(s) (Wissel *et al*., 2005). We tested these ideas by generating a *gfp* fusion to the *C. crescentus ftsI* sequence encoding the N-terminal 90-residue sequence of *C. crescentus* PBP3. This fusion was designed to encode the cytoplasmic region (which is slightly longer than that of *E. coli* PBP3), the TM segment and the next 26 periplasmic residues of *C. crescentus* PBP3. This fusion displayed no discernible ring-like localization in the merodiploid strain carrying wild-type *ftsI* (Fig. 6A) or in the *ftsI*(Ts) mutant at either permissive or restrictive temperatures (Fig. 6B). Biochemical fractionation followed by immunoblotting (using GFP antibody) verified membrane attachment (Fig. 6C). The appearance of degradation products suggested that the GFP–PBP3$_{1–90}$ fusion was not fully stable. However, the products, including the smallest detectable one (asterisk, Fig. 6C), was membrane-bound, suggesting that the TM segment was present. The absence of ring-like localization (Fig. 6A and B) therefore argues that the TM sequence of PBP3 is not a major targeting determinant in *C. crescentus*.

A role for PBP3 catalytic activity in localization has been previously suggested based on the observation that treatment of *E. coli* with β-lactam antibiotics such as cephalexin and aztreonam that specifically block PBP3 transpeptidase activity affects PBP3 localization (Wang *et al*., 1998). However, later studies show that the localization of PBP3 is unaffected by similar drug treatments (Weiss *et al*., 1999; Den Blaauwen *et al*., 2003; Bertsche *et al*., 2006). We could not use cephalexin for our studies because this antibiotic displayed a broader spectrum of activity in *C. crescentus*, inhibiting binding of a fluorescent penicillin derivative (BOCILLIN-FL) to several PBPs at a similar level when added at concentrations that induce cell filamentation (Fig. S3A). This competitive binding assay was performed in a Δ*bla* strain in which the β-lactamase-encoding gene is inactivated. Aztreonam was also useless, as even *C. crescentus* Δ*bla* is resistant to it (data not shown). Instead, we used fosfomycin, which blocks PG precursors synthesis by inhibiting the MurA enzyme (Kahan *et al*., 1974). While this drug does not

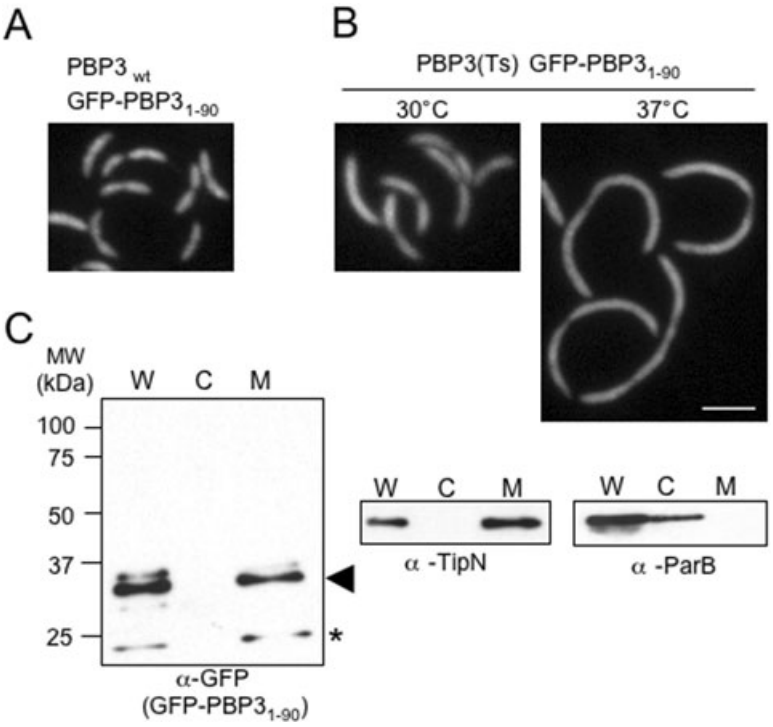

Fig. 6. The PBP3 TM segment is not sufficient for ring-like localization.
A. Fluorescence micrograph of merodiploid CJW2851 cells expressing *gfp–ftsI*$_{1–90}$ for 4 h in xylose medium.
B. Fluorescence micrographs of CJW2852 cells carrying *ftsI*(Ts) and *gfp–ftsI*$_{1–90}$. After 4 h of growth in xylose at 30°C, the cultures were split and incubated for an additional 2 h at 30°C or 37°C before imaging. Scale bar, 2 μm.
C. Immunoblot analysis of biochemically fractionated samples from CJW2851 cells (CB15N *Pxyl*::*Pxyl–gfp–ftsI*$_{1–90}$) grown in the presence of xylose for 6 h (to produce GFP–PBP3$_{1–90}$). Arrowhead and asterisk show products. W, whole-cell extract; C, cytoplasmic fraction; M, membrane fraction; MW, molecular weight markers.

© 2008 The Authors

block PBP3 activity *per se*, it should ultimately reduce the availability of PBP3 substrates. CJW1823 cells (CB15N *Pxyl*::*Pxyl–gfp–ftsI Pvan*::*Pvan–ftsZ–mCherry*) producing GFP–PBP3 and FtsZ–mCherry were treated with 40 μg ml^{-1} of fosfomycin. Under these conditions, cell growth was arrested after 3 h of exposure (data not shown), suggesting a substantial depletion of PG precursors. The localization of GFP–PBP3 was quantified relative to FtsZ–mCherry rings, which served as a spatial reference. Without drug treatment, GFP–PBP3 accumulation at the pole and colocalization with FtsZ–mCherry were not impaired; however, after 3 h of fosfomycin treatment, the polar localization of PBP3 and its colocalization with FtsZ–mCherry were both appreciably reduced (Fig. S3B). It is likely that the pool of PG precursors was not completely depleted under the conditions used (which would be difficult to achieve without inducing significant cell lysis). Regardless, our results showed that reduction of PG precursors, which ultimately leads to a reduction of glycan strand incorporation and thus PBP3 substrates, is accompanied with a small but noticeable decrease in PBP3 localization.

A more conclusive way to address the role of transpeptidase activity in PBP3 localization was to disrupt the catalytic site of PBP3 by mutation. By sequence alignment, the active site of *C. crescentus* PBP3 was identified as serine-296, which corresponds to serine-307 in *E. coli* PBP3 (Houba-Herin *et al*., 1985; Nicholas *et al*., 1985). An *ftsI* allele creating a S296A substitution was fused to *gfp* and placed under *Pxyl*. Consistent with an inactivation of the catalytic site, production of GFP–PBP3$_{S296A}$ did not complement the *ftsI*(Ts) allele at 37°C in cells [CJW2236, CB15N *ftsI*(Ts) *Pxyl*::*Pxyl–gfp–ftsI*$_{S296A}$] grown in xylose (Fig. 7A). Next, we examined the localization of inactive GFP–PBP3$_{S296A}$ in cells (CJW2237, CB15N *Pxyl*::*Pxyl–gfp–ftsI*$_{S296A}$ *Pvan*::*Pvan–ftsZ–mCherry*) that also produced FtsZ–mCherry (to serve as a spatial reference). We used synchronized swarmer and pre-divisional cell populations, which, for wild-type PBP3, predominantly exhibit a polar and medial localization respectively. While medial FtsZ–mCherry localization was normal, the percentage of swarmer and pre-divisional cells with polar and medial GFP–PBP3$_{S296A}$ localization was significantly reduced (Fig. 7B and C). PBP3 is thought to dimerize (Broome-Smith *et al*., 1985; Weiss *et al*., 1999; Marrec-Fairley *et al*., 2000; Wissel and Weiss, 2004), raising the possibility that the residual localization of GFP–PBP3$_{S296A}$ might be in part due to heterodimer formation between GFP–PBP3$_{S296A}$ and wild-type PBP3.

We therefore moved the *ftsI*$_{S296A}$ allele into the *ftsI*(Ts) mutant background [CJW2236, CB15N *ftsI*(Ts) *Pxyl*::*Pxyl–gfp–ftsI*$_{S296A}$]. Immunoblot analysis revealed that at both 30°C and 37°C, GFP–PBP3$_{S296A}$ accumulated to a lower steady-state level than wild-type GFP–PBP3 under the same xylose-inducing conditions (Fig. S1, lanes 5 and 6 compared with lanes 1 and 3). This decrease in GFP–PBP3$_{S296A}$ levels was also observed when cells expressed a wild-type allele of *ftsI* [instead of *ftsI*(Ts)] (Fig. S1, lane 8 compared with lane 7), suggesting that the functionality of the catalytic site is important for protein stability. We do not believe that this defect affected our ability to examine the localization of GFP–PBP3$_{S296A}$, because in all cases (irrespective of temperature or *ftsI* background), the levels of xylose-induced GFP–PBP3$_{S296A}$ were well above those of an endogenously expressed GFP–PBP3 (Fig. S1, lanes 5, 6 and 8 compared with lane 9) whose medial and polar localizations were readily detectable (Fig. 3). Consistent with this inference, synthesis of GFP–PBP3$_{S296A}$ in the *ftsI*(Ts) background at 30°C resulted in one or two strong fluorescent bands in all cells that were observed (100%, $n = 168$) (Fig. 7D and E). While this clearly indicates that the steady-state level of GFP–PBP3$_{S296A}$ is not a problem for visualizing localization, it was surprising that the localization of GFP–PBP3$_{S296A}$ was enhanced when the PBP3(Ts) mutant was present instead of wild-type PBP3. This was accompanied by a dominant effect on cell division as most cells were noticeably elongated (Fig. 7A).

At 37°C when the function of the PBP3(Ts) mutant was abrogated and all cells were filamentous, only about 20% and 3% of cells displayed one or two bands of GFP–PBP3$_{S296A}$ respectively (Fig. 7D and E). Thus, in total, GFP–PBP3$_{S296A}$ exhibited a band-like localization in only about 23% of *ftsI*(Ts) cells at 37°C. Even in these cases, the localization signal was considerably weaker than that at 30°C (arrow, Fig. 7D). The steady-state level of GFP–PBP3$_{S296A}$ at 37°C is similar to that at 30°C at which temperature, band localization is readily discernible in all cells (Fig. S1, lane 6 versus lane 5), indicating that the localization defects at 37°C are not caused by the cellular levels of GFP–PBP3$_{S296A}$. Instead, they argue that the active site of PBP3 plays an important role in PBP3 localization.

This interpretation stands only if FtsZ rings are able to form in *ftsI*(Ts) cells at 37°C, as they do in *E. coli* (Addinall *et al*., 1996). Otherwise, impairment in FtsZ ring formation would explain the localization defect of GFP–PBP3$_{S296A}$ at 37°C. To verify that FtsZ rings form in the absence of functional PBP3 in *C. crescentus*, we examined FtsZ–YFP localization in *ftsI*(Ts) cells [CJW2577, CB15N *ftsI*(Ts) *Pvan*::*Pvan–ftsZ–yfp*] after incubation at 37°C. Over 90% of these filamentous *ftsI*(Ts) cells ($n = 95$) formed one or more FtsZ–YFP rings (Fig. 7E and F). About 29% of these cells had two rings per cell, while 10% and 6% of the cells displayed three and four (or more) rings respectively (data not shown). Thus, FtsZ can still

© 2008 The Authors
Journal compilation © 2008 Blackwell Publishing Ltd,

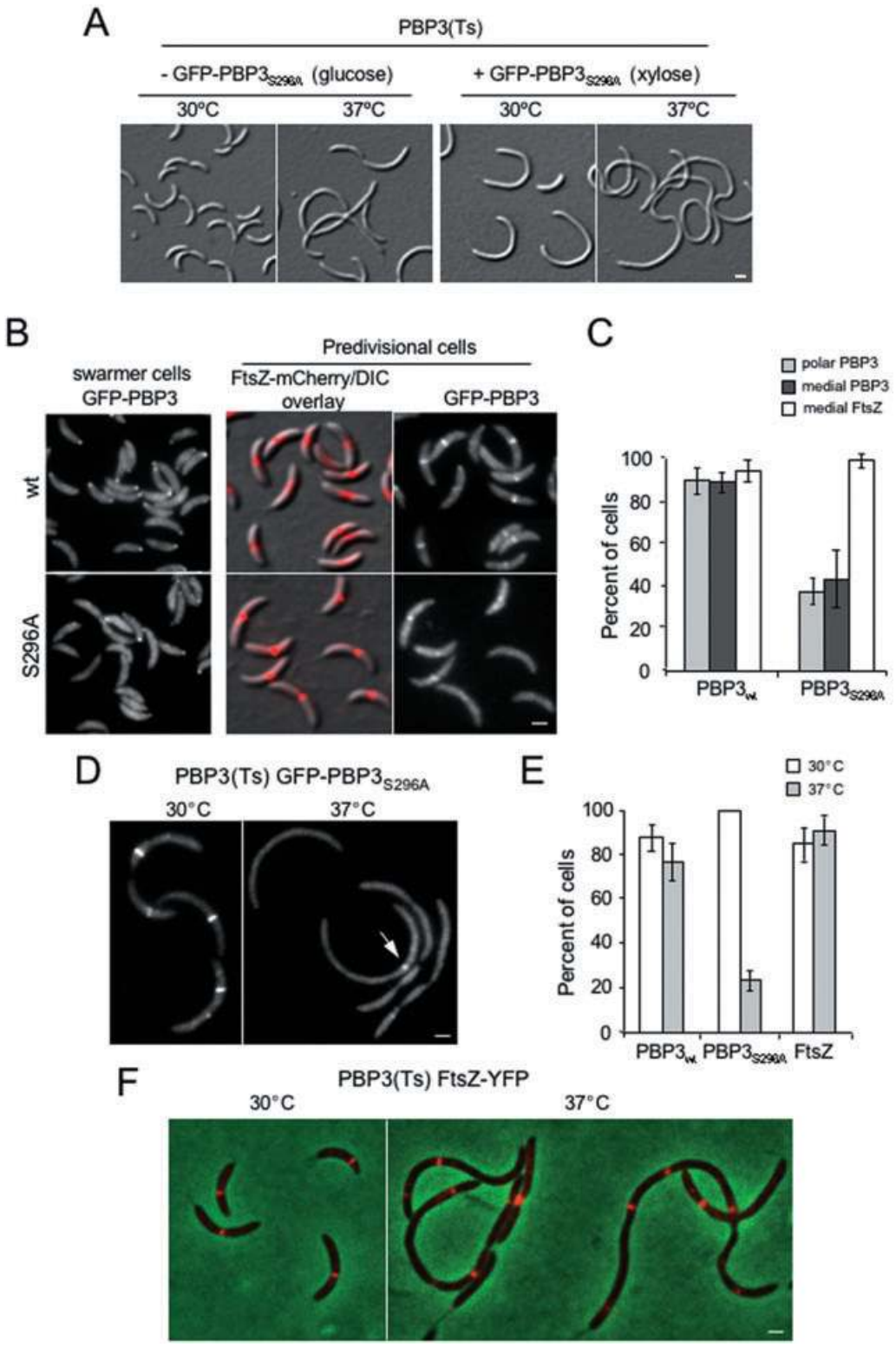

form rings in the absence of functional PBP3. In contrast, abolition of functional PBP3 dramatically reduces the localization of the catalytically inactive $PBP3_{S296A}$ mutant, both in percentage of cells with band-like localization and in signal intensity (relative to its signal at 30°C). These observations suggest that in *C. crescentus*, the localization of PBP3 relies in large part on a functional PBP3 transpeptidase domain.

© 2008 The Authors
Journal compilation © 2008 Blackwell Publishing Ltd,

Fig. 7. The catalytic site of PBP3 is important for PBP3 localization.
A. The inactive PBP3$_{S296A}$ mutant does not support PBP3 function and confers a dominant-negative effect on the function of the PBP3(Ts) mutant at the permissive temperature. CJW2236 cultures [CB15N *ftsI*(Ts) *Pxyl*::*Pxyl–gfp–ftsI*$_{S296A}$], carrying the *ftsI*(Ts) mutation and xylose-inducible *gfp–ftsI*$_{S296A}$, were first grown at 30°C. Samples were used to inoculate fresh media and the resulting cultures were incubated at either 30°C or 37°C for 3 h. The cultures were kept in log-phase. GFP–PBP3$_{S296A}$ was unable to complement the *ftsI*(Ts) filamentous phenotype after 3 h of incubation at 37°C. Even at 30°C, CJW2236 cells producing GFP–PBP3$_{S296A}$ (xylose conditions) were noticeably elongated, suggestive of a dominant-negative effect of GFP–PBP3$_{S296A}$ on PBP3(Ts) function, likely due to PBP3 dimerization.
B. The S296A mutation impairs the ability of PBP3 to localize at the pole and to the FtsZ ring. CJW1823 cells (CB15N *Pxyl*::*Pxyl–gfp–ftsI Pvan*::*Pvan–ftsZ–mcherry*) and CJW2137 cells (CB15N *Pxyl*::*Pxyl–gfp–ftsI*$_{S296A}$ *Pvan*::*Pvan–ftsZ–mcherry*), which still produce wild-type PBP3 from its native locus, were incubated for 2 h in vanillic acid and 6 h in xylose (to induce the synthesis of FtsZ–mCherry and GFP–PBP3 or GFP–PBP3$_{S296A}$) prior to synchrony. The localization of FtsZ–mCherry and GFP–PBP3 or GFP–PBP3$_{S296A}$ was examined in swarmer and pre-divisional cells collected at 0 and 60 min after synchrony respectively. FtsZ–mCherry localization in pre-divisional cells, which serves as a positioning reference, is shown in an overlay of fluorescence (red) and DIC images. The corresponding GFP–PBP3 or GFP–PBP3$_{S296A}$ images are shown on the right. Scale bar, 1 μm.
C. Quantitative analysis of (B). At least 190 cells of CJW1823 and CJW2137 strains from three separate microscopy experiments were analysed. Polar and medial localization patterns were examined in synchronized swarmer and pre-divisional cell populations respectively.
D. GFP–PBP3$_{S296A}$ localization is severely disrupted in the absence of a functional copy of PBP3. CJW2236 cells [CB15N *ftsI*(Ts) *Pxyl*::*Pxyl–gfp–ftsI*$_{S296A}$] carrying *ftsI*(Ts) and *gfp–ftsI*$_{S296A}$ were used to inoculate fresh media containing xylose. The resulting cultures were incubated for 3 h at 30°C. The cultures were then split and incubated for an additional 1.5 h at 30°C or 37°C. GFP–PBP3$_{S296A}$ fluorescent microscopy images are shown. Arrow shows residual localization of GFP–PBP3$_{S296A}$. Scale bar, 1 μm.
E. Quantitative analysis of (D) and (F). At least 100 cells of CJW2235, CJW2236 and CJW2577 strains from three separate microscopy experiments were analysed. Per cent of cells showing a band or focus of GFP–PBP3 (PBP3$_{wt}$), GFP–PBP3$_{S296A}$ (PBP3$_{S296A}$) and FtsZ–YFP (FtsZ) in *ftsI*(Ts) cells grown at 30°C or 37°C are shown.
F. FtsZ–YFP forms bands in *ftsI*(Ts) cells. A CJW2577 culture [CB15N *ftsI*(Ts) *Pvan*::*Pvan–ftsZ–yfp*] was used to inoculate fresh PYE media containing vanillic acid and the resulting cultures were incubated for 2 h at 30°C. The cultures were then split and incubated for 1.5 h at 30°C or 37°C. The cells were fixed with 2.5% formaldehyde before microscopy. Overlaid images of phase contrast (green) and FtsZ–YFP fluorescence (red) are shown. Scale bar, 1 μm.

Discussion

Temporal changes in PBP3 subpopulations

PBP3 localization varies during the cell cycle. At the beginning of the cell cycle, PBP3 accumulates at the new cell pole, creating a polar pool. Polar localization of PBP3 has also been reported in *E. coli* in one immunofluorescence microscopy study (Weiss *et al*., 1997). Later, using fluorescence microscopy and GFP tagging, polar localization of *E. coli* PBP3 was only observed when the protein was overproduced by 10-fold suggesting to the authors that previous observations of polar PBP3 may have been artificially produced (Weiss *et al*., 1999). In *C. crescentus*, polar accumulation is also observed when GFP–PBP3 is produced under native conditions (Fig. 3).

Later during the cell cycle, the polar accumulation of PBP3 disappears concomitantly with the re-localization of PBP3 to the FtsZ ring, generating a medial pool; this event is FtsZ-dependent. PBP3 and FtsZ remain colocalized throughout the constriction process that leads to the formation of new cell poles. Interestingly, there is also a portion of PBP3 molecules diffusely dispersed around the membrane at all times (i.e. during both cell elongation and division). The FRAP experiments demonstrate that this membranal pool of PBP3 is not static as it rapidly exchanges PBP3 molecules with the polar and medial pools, presumably through diffusion.

A role for a functional transpeptidase domain in PBP3 localization

A number of studies have suggested that PBP3 interactions with other divisomal proteins are important for PBP3 localization at midcell (den Blaauwen *et al*., 2008). Such interactions are likely responsible for the residual localization of the inactive PBP3$_{S296A}$ mutant in the filamentous *ftsI*(Ts) cells (Fig. 7D and E). This suggests that PBP3 localization is mediated by both protein–protein interaction and covalent substrate binding during transpeptidation, with the latter mechanism being responsible for the large localization defect of the catalytic site mutant. A similar substrate-driven mechanism of localization has been proposed for other PBPs in some Gram-positive bacteria (Morlot *et al*., 2004; Pinho and Errington, 2005). Alternatively, in *C. crescentus*, the interaction of PBP3 with its target protein(s) might be under allosteric regulation such that it might be favoured when the PBP3 enzyme is active. This does not appear to be the case in *E. coli* where a short N-terminal PBP3 fragment that includes the TM region is sufficient to mediate septal localization (Piette *et al*., 2004; Wissel *et al*., 2005). The observation that the TM sequence fails to localize in *C. crescentus* is consistent with its poor sequence conservation among bacteria and highlights the importance of studying homologues from different species.

Assembly of the mature divisome is thought to occur in two steps (Aarsman *et al*., 2005). First, FtsZ and early-division proteins assemble, and then, after a notable delay, PBP3 and other late-division proteins are simultaneously recruited to the FtsZ ring to form the mature divisome. Kymograph analysis of the relative spatial distribution of PBP3 and FtsZ during the *C. crescentus* cell cycle confirms the existence of a delay between FtsZ ring

© 2008 The Authors
Journal compilation © 2008 Blackwell Publishing Ltd,

assembly and the start of PBP3 accumulation at the FtsZ ring. Interestingly, the initiation of PBP3 accumulation near midcell corresponds to about the time when the FtsZ ring stabilizes at one position.

The kymographs also demonstrate that the recruitment of PBP3 to the FtsZ ring is initiated well before cell constriction begins, and is very gradual, spanning a considerable part of the elongation phase (Figs 2B and 3B). What drives this slow and early accumulation of PBP3 at the FtsZ ring? The fact that this gradual accumulation is observed whether the GFP–PBP3 fusion is under native cell cycle-controlled synthesis (Fig. 3) or under constitutive production (Fig. 2) rules out the possibility that this is due to transcriptional control. The FRAP measurements of GFP–PBP3 dynamics clearly indicate that membrane diffusion is very rapid (Fig. 5 and Fig. S2), as previously demonstrated for other membrane-bound proteins (Deich *et al*., 2004; Mullineaux *et al*., 2006). Therefore, the progressive recruitment of PBP3 to the divisome is not limited by PBP3 diffusion. Instead, it may be caused by a slow and early accumulation of an upstream interacting division protein. Alternatively, it may be driven by the accumulation of PBP3 substrates. It is known that shortly after its formation, the FtsZ ring largely redirects PG synthesis near midcell (Aaron *et al*., 2007). PG synthesis at the FtsZ ring position may thus recruit PBP3 at this location by generating substrates for PBP3. Interactions with other divisomal proteins may then strengthen PBP3 localization. In this scenario, the gradual accumulation of PBP3 at the FtsZ ring would result from two competing sites that are rich in PBP3 substrates: the FtsZ ring location where new substrates are being produced, and the new pole where PBP3 substrates may remain from the previous division. Without repletion of PBP3 substrates, the polar site may slowly lose its ability to recruit PBP3 compared with the FtsZ ring site over time, causing a gradual accumulation of PBP3 at the FtsZ ring location.

Using short-lived complexes for PG synthesis

Our FRAP experiments reveal that PBP3 molecules at the division site are continuously being exchanged with PBP3 present in the membrane pool, and this exchange occurs within seconds. Compared with this time scale, the formation of poles during division is a very long process. This indicates that septal PG synthesis is not achieved by the same mature divisome complexes. Instead, the contribution of any one specific PBP3-containing complex to septal PG synthesis is very short-lived.

A role for PBP3 at the new pole?

The FRAP experiments also demonstrate that the accumulation of PBP3 at the new pole of newborn cells does not correspond to a remnant from the previous cell division given the rapid and FtsZ-independent exchange of PBP3 between polar and membrane pools. This might mean that after division, PBP3 continues performing transpeptidation (cross-linking) reactions at the new pole for a significant period of time. Division in *C. crescentus* generates hemispherical poles, which become gradually more pointed following division (Aaron *et al*., 2007). This morphological pole maturation event must involve PG synthesis or remodelling, and the polar PBP3 activity may contribute to this activity. We unsuccessfully attempted to test this hypothesis by using the *ftsI*(Ts) mutant (data not shown). The loss of PBP3 activity appeared to be too gradual and not immediate enough following temperature shift to provide useful information. Examining the role of PBP3 localization at the pole might require obtaining mutations or conditions that allow PBP3 targeting to the divisome while impairing its localization to the pole. As far as we can tell, there is no evidence to suggest that these two localization events use different mechanisms, suggesting that it might be difficult to uncouple them. Interestingly, it has been reported that a single amino acid substitution (N361S) in PBP3 generates *E. coli* cells with pointed poles (Taschner *et al*., 1988). We found that in this *E. coli* mutant, the formation of pointed poles occurs during cell division (Movie S1) and not following division, as is observed in wild-type *C. crescentus* (Aaron *et al*., 2007).

Experimental procedures

Bacterial strains, plasmids and growth conditions

Strains and plasmids are listed in Table 1 and their mode of construction is provided in *Supporting information*. Plasmids were constructed using the *E. coli* strains DH5α and S17-1, routinely grown in LB medium at 37°C with appropriate antibiotic selection. *C. crescentus* strains were grown at 30°C or 37°C [restrictive temperature for the *ftsI*(Ts) mutant] to log-phase in rich PYE medium or minimal M2G medium supplemented with 1% PYE ($M2G^+$) (Ely, 1991). *C. crescentus* was genetically manipulated by transformation, conjugation and transduction as previously described (Ely, 1991). Synchronous cell populations were obtained as previously described (Evinger and Agabian, 1977). Expression from *Pxyl* or *Pvan* was achieved by adding 0.3% xylose or 0.5 mM vanillic acid to the medium when indicated.

Light microscopy

For time-course experiments, swarmer cells were incubated at 30°C in liquid PYE medium (containing xylose, glucose or vanillic acid as appropriate) to resume growth. At specific time intervals, an aliquot of the culture was taken. The cells were then washed in $M2G^+$ medium and visualized on agarose-padded slides containing $M2G^+$ medium.

© 2008 The Authors
Journal compilation © 2008 Blackwell Publishing Ltd,

Table 1. Strains and plasmids.

Strain/plasmid	Relevant genotype or description	Reference or source
Strain		
C. crescentus		
CJW27	CB15N (or NA1000), synchronizable variant of CB15	Evinger and Agabian (1977)
CJW1438	CB15N *vanA*::pMT400	M. Thanbichler and L. Shapiro
CJW1497	CB15N Δ*bla*	West *et al.* (2002)
CJW1472	CB15N *xylX*::pGFP4C1	A.F. Jackson
CJW1550	CB15N *vanA*::pNJH17	M. Thanbichler, N. Hillson and L. Shapiro
CJW1822	CB15N *xylX*::pTC34-3	This work
CJW1823	CB15N *vanA*::pNJH17 *xylX*::pTC34-3	This work
CJW2136	CB15N *xylX*::pTC49	This work
CJW2137	CB15N *vanA*::pNJH17 *xylX*::pTC49	This work
CJW2141	CB15N *cc2570*::pTC67 *ftsI*(Ts)	This work
CJW2142	CB15 *divA*305 str-179 *cc2570*::pTC67	This work
CJW2143	CB15N *ftsI*::pTC71 *ftsZ*::pBJM1	This work
CJW2144	CB15N *ftsI*::pTC71	This work
CJW2235	CB15N *cc2570*::pTC67 *ftsI*(Ts) *xylX*::pTC34-3	This work
CJW2236	CB15N *cc2570*::pTC67 *ftsI*(Ts) *xylX*::pTC49	This work
CJW2577	CB15N *cc2570*::pTC67 *ftsI*(Ts) *vanA*::pMT400	This work
CJW2851	CB15N *xylX*::pRP3	This work
CJW2852	CB15N *cc2570*::pTC67 *ftsI*(Ts) *xylX*::pRP3	This work
PC7167	CB15 *divA*305 str-179 [*ftsI*(Ts)]	Ohta *et al.* (1997)
YB1585	CB15N *ftsZ*::pBJM1	Wang *et al.* (2001)
E. coli		
CJW1820	DH5α/pTC34-3	This work
CJW1821	S17-1/pTC34-3	This work
CJW2127	S17-1/pTC49	This work
CJW2130	S17-1/pTC67	This work
CJW2131	DH5α/pTC71	This work
CJW2850	DH5α/pRP3	This work
DH5a	Cloning strain	Invitrogen
S17-1	RP4-2, Tc::Mu, KM-Tn*7*, for plasmid mobilization	Simon *et al.* (1983)
Plasmids		
pBJM1	pBGST18T carrying the *xylX* promoter (*Pxyl*) and 489 bp from the 5′ end of *ftsZ*	Wang *et al.* (2001)
pMT400	Apr^R integration vector carrying *ftsZ–yfp* under the control of the vanillate-inducible promoter (*Pvan*)	M. Thanbichler and L. Shapiro
pNHJ17	Gent^R integration vector carrying *ftsZ–mcherry* under the control of *Pvan*	M. Thanbichler, N. Hillson and L. Shapiro
pRP3	Kan^R integration vector carrying *gfp–ftsI*$_{1–90}$ under the control of *Pxyl*	This work
pTC34-3	Kan^R integration vector carrying *gfp–ftsI* under the control of *Pxyl*	This work
pTC49	Kan^R integration vector carrying *gfp–ftsI*$_{S296A}$ under *Pxyl*	This work
pTC67	Gent^R integration vector carrying 512 bp of the 5′ end of *cc*2570 coding sequence, including 162 bp upstream ATG start codon. Insertion at *cc2570* locus restores a wt *cc2570* gene copy	This work
pTC71	pNPTS138 carrying *gfp–ftsI*	This work
pXGFP4C1	Kan^R integration vector carrying *gfp* under the control of *Pxyl*	Gitai *et al.* (2004)
pNPTS138	Kan^R integrational vector carrying the *sacB* gene that allows plasmid remova after integration. Limus38 derivative	M.R.K. Alley

For time-lapse experiments, cells were observed on slides padded with 1% agarose in M2G$^+$ medium supplemented with 0.3% xylose and 0.5 mM vanillic acid. Time-lapse experiments with *C. crescentus* and *E. coli* were performed at room temperature and 37°C respectively. Kymographs were constructed using MetaMorph Software to display the maximum intensity values of fluorescent signals along the length of a 3-μm-wide region across the long axis of the cell as a function of time.

Samples were observed on a Nikon E1000 microscope equipped with Hamamatsu Orca-ER camera, differential interference contrast (DIC) and phase-contrast 100× objectives, and standard filter sets for visualization of GFP, YFP and mCherry. Image acquisition was performed using MetaMorph software (MDS Analytical Technologies). When appropriate, a heated objective was used. Quantitative analysis of protein localization was performed visually on still images.

Fluorescence recovery after photobleaching

FRAP experiments were performed using a Nikon Eclipse 80i microscope equipped with an Andor iXon^{EM}+ (DU-897E) EMCCD camera and a galvanometer-controlled Photonic Instruments MicroPoint laser. Cells cultures immobilized on 1.5% agarose-padded slides containing M2G$^+$ medium were observed with a DIC 100× objective, 2× magnification optivar and standard filter sets. Photobleaching was achieved using

© 2008 The Authors
Journal compilation © 2008 Blackwell Publishing Ltd,

two pulses of 37 ms with 30% laser intensity, which was additionally attenuated by using external attenuator set to 2 and the attenuation plate set to 45, plus a ND16 filter. Images were collected before photobleaching (pre-bleach), immediately after bleaching and at 5–10 s intervals after bleaching for 2 min. Measurements of integrated fluorescence intensity in the bleached or unbleached regions, as well as whole-cell intensity, were obtained at each time point with MetaMorph and exported to Excel. For each measured region, background intensity was subtracted and the fluorescent signal normalized for photobleaching occurring during image acquisition (by measuring the fluorescence decay in unbleached neighbouring cells). The averaged pre-bleach fluorescence intensity was normalized to 100% by dividing the averaged intensity of all time points by the averaged pre-bleach intensity. All analysed samples were found to fit a normally distributed population with a 99% confidence interval. Recovery half-times were determined by performing a least-squared fit of the intensity of the bleached region over time to the single-exponential equation $F(t) = A(1 - e^{-B*t})$, where $F(t)$ is the fluorescence at time t, A is the maximum intensity and B the slope. Least-squared fits were performed in Excel using the Solver function. All obtained fitting curves showed $r^2 \geq 0.95$. Half-time recovery values were determined by the formula $t_{1/2} = \ln(0.5)/-B$ and the standard deviation was calculated using the SETXY formula of Excel. Data were collected for over 23 cells from at least two independent time-lapse experiments. After the completion of the FRAP experiments, control time-lapse experiments were performed to ensure that the photobleached cells grew and divided. To test recovery under conditions in which protein synthesis is blocked, *gfp–ftsI* expression was repressed by incubating the cells in 0.2% glucose for 30 min, then 20 μg ml^{-1} chloramphenicol (CAM) was added for 20 min, and then the cells were placed on M2G^{+} agarose-padded slides containing 20 μg ml^{-1} CAM. The whole-cell intensity was shown to remain constant for 60 min under these conditions.

Biochemical fractionation

After growth, cells were harvested and re-suspended in 50 mM sodium phosphate buffer (pH 7.4) containing 50 mM NaCl, 1 mM EDTA and 1× protease inhibitor cocktail (Roche). Whole-cell lysates were prepared by sonication and 0.3 ml of lysates were centrifuged at 14 000 r.p.m. for 10 min at 4°C or prepared by French pressed at 1500 psi and the cell lysate was centrifuged at 10 000 r.p.m. for 15 min at 4°C. The supernatant constituted the whole-cell lysate. All whole-cell lysates were then centrifuged at 120 000 r.p.m. in a TLA100.2 rotor for 1 h at 4°C using an Optima TLX ultracentrifuge (Beckman Coulter). The supernatant, corresponding to the cytoplasmic fraction, was collected while the pellet was re-suspended in 0.3 ml of the same phosphate buffer to produce the membrane fraction.

Immunoblot analysis

For immunoblot analysis of cell extracts, 3 ml of cultures grown under appropriate conditions were collected and the whole-cell lysates prepared by sonication. Thirty micrograms (15 μg for biochemical fractionation) of total protein was electrophoretically resolved on 12% SDS-PAGE gels, and the resolved proteins were electrotransferred to PVDF membranes, which were probed with anti-GFP (1:1000; Clontech), anti-ParB (1:4000) (Mohl and Gober, 1997) and anti-TipN (1:12 500) antibodies (Lam *et al.*, 2006)

BOCILLIN-FL assays

BOCILLIN-FL competition binding assays were performed from late-log-phase cultures ($A_{660} = 0.5–0.8$). Cells were first lysed by treatment with 100 μg ml^{-1} lysozyme in the presence of 10 U DNase I, and centrifuged. The membrane-enriched fraction (insoluble fraction) was re-suspended in a buffer (100 mM Tris-HCl pH 7.5, 1 mM EDTA pH 8.0) containing increasing amounts of cephalexin. Samples were incubated for 45 min at 30°C, washed and incubated under similar conditions with 10 μM BOCILLIN-FL, a fluorescent derivative of penicillin (Molecular Probes). Samples were then washed and the proteins separated by electrophoresis on 10% SDS-PAGE gels. BOCILLIN-FL-bound proteins were observed using a Typhoon imager Trio+ (Molecular Dynamics, Amersham Biosciences) under excitation and emission of 488 and 532 nm respectively. A large excess of penicillin G, which competes with BOCILLIN-FL, was used as a specificity control for the identification of PBPs.

Acknowledgements

We thank A.F. Jackson, N. Ohta, A. Newton, Y.V. Brun, P. Taschner, M. Thanbichler and L. Shapiro for providing strains, M. Mooseker for the use of his Ultracentrifuge, R. Breaker for the use of his Typhoon scanner, W. Vollmer and T. Emonet for valuable discussions, S. Poggio and P. Montero for their help with the sonication, and W. Vollmer and all members of the Jacobs-Wagner laboratory for critical reading of the manuscript. This work was supported by Anderson Postdoctoral Fellowships (to R.P. and T.C.), Fellowship SFRH/PBD/26232/2006 from 'Fundação para a Ciência e a Tecnologia' (to T.C.), National Institutes of Health Grants GM076698 and GM065835 (to C.J.-W.) and the Pew Charitable Trusts (to C.J.-W.). C.J.-W. is a Howard Hughes Medical Institute Investigator.

References

Aaron, M., Charbon, G., Lam, H., Schwarz, H., Vollmer, W., and Jacobs-Wagner, C. (2007) The tubulin homologue FtsZ contributes to cell elongation by guiding cell wall precursor synthesis in *Caulobacter crescentus*. *Mol Microbiol* **64:** 938–952.

Aarsman, M.E., Piette, A., Fraipont, C., Vinkenvleugel, T.M., Nguyen-Distèche, M., and den Blaauwen, T. (2005) Maturation of the *Escherichia coli* divisome occurs in two steps. *Mol Microbiol* **55:** 1631–1645.

Addinall, S.G., Bi, E., and Lutkenhaus, J. (1996) FtsZ ring formation in *fts* mutants. *J Bacteriol* **178:** 3877–3884.

Bertsche, U., Kast, T., Wolf, B., Fraipont, C., Aarsman, M.E., Kannenberg, K., *et al.* (2006) Interaction between two murein (peptidoglycan) synthases, PBP3 and PBP1B, in *Escherichia coli*. *Mol Microbiol* **61:** 675–690.

© 2008 The Authors

den Blaauwen, T., de Pedro, M.A., Nguyen-Distèche, M., and Ayala, J.A. (2008) Morphogenesis of rod-shaped sacculi. *FEMS Microbiol Rev* **32:** 321–344.

Bowler, L.D., and Spratt, B.G. (1989) Membrane topology of penicillin-binding protein 3 of *Escherichia coli*. *Mol Microbiol* **3:** 1277–1286.

Broome-Smith, J.K., Hedge, P.J., and Spratt, B.G. (1985) Production of thiol-penicillin-binding protein 3 of *Escherichia coli* using a two primer method of site-directed mutagenesis. *EMBO J* **4:** 231–235.

Cabeen, M.T., and Jacobs-Wagner, C. (2005) Bacterial cell shape. *Nat Rev Microbiol* **3:** 601–610.

Corbin, B.D., Geissler, B., Sadasivam, M., and Margolin, W. (2004) Z-ring-independent interaction between a subdomain of FtsA and late septation proteins as revealed by a polar recruitment assay. *J Bacteriol* **186:** 7736–7744.

Curtis, N.A., Eisenstadt, R.L., Turner, K.A., and White, A.J. (1985) Inhibition of penicillin-binding protein 3 of *Escherichia coli* K-12. Effects upon growth, viability and outer membrane barrier function. *J Antimicrob Chemother* **16:** 287–296.

Deich, J., Judd, E.M., McAdams, H.H., and Moerner, W.E. (2004) Visualization of the movement of single histidine kinase molecules in live *Caulobacter* cells. *Proc Natl Acad Sci USA* **101:** 15921–15926.

Den Blaauwen, T., Buddelmeijer, N., Aarsman, M.E., Hameete, C.M., and Nanninga, N. (1999) Timing of FtsZ assembly in *Escherichia coli*. *J Bacteriol* **181:** 5167–5175.

Den Blaauwen, T., Aarsman, M.E., Vischer, N.O., and Nanninga, N. (2003) Penicillin-binding protein PBP2 of *Escherichia coli* localizes preferentially in the lateral wall and at mid-cell in comparison with the old cell pole. *Mol Microbiol* **47:** 539–547.

Derouaux, A., Wolf, B., Fraipont, C., Breukink, E., Nguyen-Distèche, M., and Terrak, M. (2008) The monofunctional glycosyltransferase of *Escherichia coli* localizes to the cell division site and interacts with penicillin-binding protein 3, FtsW, and FtsN. *J Bacteriol* **190:** 1831–1834.

Di Lallo, G., Fagioli, M., Barionovi, D., Ghelardini, P., and Paolozzi, L. (2003) Use of a two-hybrid assay to study the assembly of a complex multicomponent protein machinery: bacterial septosome differentiation. *Microbiology* **149:** 3353–3359.

Divakaruni, A.V., Baida, C., White, C.L., and Gober, J.W. (2007) The cell shape proteins MreB and MreC control cell morphogenesis by positioning cell wall synthetic complexes. *Mol Microbiol* **66:** 174–188.

Ely, B. (1991) Genetics of *Caulobacter crescentus*. *Methods Enzymol* **204:** 372–384.

Errington, J., Daniel, R.A., and Scheffers, D.J. (2003) Cytokinesis in bacteria. *Microbiol Mol Biol Rev* **67:** 52–65.

Evinger, M., and Agabian, N. (1977) Envelope-associated nucleoid from *Caulobacter crescentus* stalked and swarmer cells. *J Bacteriol* **132:** 294–301.

Gitai, Z., Dye, N., and Shapiro, L. (2004) An actin-like gene can determine cell polarity in bacteria. *Proc Natl Acad Sci USA* **101:** 8643–8648.

Goehring, N.W., and Beckwith, J. (2005) Diverse paths to midcell: assembly of the bacterial cell division machinery. *Curr Biol* **15:** R514–R526.

Goehring, N.W., Gonzalez, M.D., and Beckwith, J. (2006) Premature targeting of cell division proteins to midcell reveals hierarchies of protein interactions involved in divisome assembly. *Mol Microbiol* **61:** 33–45.

Goffin, C., and Ghuysen, J.M. (1998) Multimodular penicillin-binding proteins: an enigmatic family of orthologs and paralogs. *Microbiol Mol Biol Rev* **62:** 1079–1093.

Hara, H., Nishimura, Y., Kato, J., Suzuki, H., Nagasawa, H., Suzuki, A., and Hirota, Y. (1989) Genetic analyses of processing involving C-terminal cleavage in penicillin-binding protein 3 of *Escherichia coli*. *J Bacteriol* **171:** 5882–5889.

van Heijenoort, J. (1998) Assembly of the monomer unit of bacterial peptidoglycan. *Cell Mol Life Sci* **54:** 300–304.

Höltje, J.V. (1996) A hypothetical holoenzyme involved in the replication of the murein sacculus of *Escherichia coli*. *Microbiology* **142:** 1911–1918.

Höltje, J.V. (1998) Growth of the stress-bearing and shape-maintaining murein sacculus of *Escherichia coli*. *Microbiol Mol Biol Rev* **62:** 181–203.

Houba-Herin, N., Hara, H., Inouye, M., and Hirota, Y. (1985) Binding of penicillin to thiol-penicillin-binding protein 3 of *Escherichia coli*: identification of its active site. *Mol Gen Genet* **201:** 499–504.

Kahan, F.M., Kahan, J.S., Cassidy, P.J., and Kropp, H. (1974) The mechanism of action of fosfomycin (phosphonomycin). *Ann N Y Acad Sci* **235:** 364–386.

Karimova, G., Dautin, N., and Ladant, D. (2005) Interaction network among *Escherichia coli* membrane proteins involved in cell division as revealed by bacterial two-hybrid analysis. *J Bacteriol* **187:** 2233–2243.

Kelly, A.J., Sackett, M.J., Din, N., Quardokus, E., and Brun, Y.V. (1998) Cell cycle-dependent transcriptional and proteolytic regulation of FtsZ in *Caulobacter*. *Genes Dev* **12:** 880–893.

Koch, A.L. (2000) The bacterium's way for safe enlargement and division. *Appl Environ Microbiol* **66:** 3657–3663.

Kraus, W., and Höltje, J.V. (1987) Two distinct transpeptidation reactions during murein synthesis in *Escherichia coli*. *J Bacteriol* **169:** 3099–3103.

Lam, H., Schofield, W.B., and Jacobs-Wagner, C. (2006) A landmark protein essential for establishing and perpetuating the polarity of a bacterial cell. *Cell* **124:** 1011–1023.

Lutkenhaus, J. (2007) Assembly dynamics of the bacterial MinCDE system and spatial regulation of the Z ring. *Annu Rev Biochem* **76:** 539–562.

Ma, X., Ehrhardt, D.W., and Margolin, W. (1996) Colocalization of cell division proteins FtsZ and FtsA to cytoskeletal structures in living *Escherichia coli* cells by using green fluorescent protein. *Proc Natl Acad Sci USA* **93:** 12998–13003.

Marrec-Fairley, M., Piette, A., Gallet, X., Brasseur, R., Hara, H., Fraipont, C., *et al.* (2000) Differential functionalities of amphiphilic peptide segments of the cell-septation penicillin-binding protein 3 of *Escherichia coli*. *Mol Microbiol* **37:** 1019–1031.

Mercer, K.L., and Weiss, D.S. (2002) The *Escherichia coli* cell division protein FtsW is required to recruit its cognate transpeptidase, FtsI (PBP3), to the division site. *J Bacteriol* **184:** 904–912.

Mohammadi, T., Karczmarek, A., Crouvoisier, M., Bouhss, A., Mengin-Lecreulx, D., and den Blaauwen, T. (2007) The

© 2008 The Authors
Journal compilation © 2008 Blackwell Publishing Ltd,

essential peptidoglycan glycosyltransferase MurG forms a complex with proteins involved in lateral envelope growth as well as with proteins involved in cell division in *Escherichia coli*. *Mol Microbiol* **65:** 1106–1121.

Mohl, D.A., and Gober, J.W. (1997) Cell cycle-dependent polar localization of chromosome partitioning proteins in *Caulobacter crescentus*. *Cell* **88:** 675–684.

Morlot, C., Noirclerc-Savoye, M., Zapun, A., Dideberg, O., and Vernet, T. (2004) The D,D-carboxypeptidase PBP3 organizes the division process of *Streptococcus pneumoniae*. *Mol Microbiol* **51:** 1641–1648.

Mullineaux, C.W., Nenninger, A., Ray, N., and Robinson, C. (2006) Diffusion of green fluorescent protein in three cell environments in *Escherichia coli*. *J Bacteriol* **188:** 3442–3448.

Nagasawa, H., Sakagami, Y., Suzuki, A., Suzuki, H., Hara, H., and Hirota, Y. (1989) Determination of the cleavage site involved in C-terminal processing of penicillin-binding protein 3 of *Escherichia coli*. *J Bacteriol* **171:** 5890–5893.

Nakamura, M., Maruyama, I.N., Soma, M., Kato, J., Suzuki, H., and Horota, Y. (1983) On the process of cellular division in *Escherichia coli*: nucleotide sequence of the gene for penicillin-binding protein 3. *Mol Gen Genet* **191:** 1–9.

Nanninga, N. (1991) Cell division and peptidoglycan assembly in *Escherichia coli*. *Mol Microbiol* **5:** 791–795.

Nanninga, N. (1998) Morphogenesis of *Escherichia coli*. *Microbiol Mol Biol Rev* **62:** 110–129.

Nguyen-Distèche, M., Fraipont, C., Buddelmeijer, N., and Nanninga, N. (1998) The structure and function of *Escherichia coli* penicillin-binding protein 3. *Cell Mol Life Sci* **54:** 309–316.

Nicholas, R.A., Strominger, J.L., Suzuki, H., and Hirota, Y. (1985) Identification of the active site in penicillin-binding protein 3 of *Escherichia coli*. *J Bacteriol* **164:** 456–460.

Obuchowski, P.L., and Jacobs-Wagner, C. (2008) PflI, a protein involved in flagellar positioning in *Caulobacter crescentus*. *J Bacteriol* **190:** 1718–1729.

Ohta, N., Ninfa, A.J., Allaire, A., Kulick, L., and Newton, A. (1997) Identification, characterization, and chromosomal organization of cell division cycle genes in *Caulobacter crescentus*. *J Bacteriol* **179:** 2169–2180.

de Pedro, M.A., Quintela, J.C., Höltje, J.V., and Schwarz, H. (1997) Murein segregation in *Escherichia coli*. *J Bacteriol* **179:** 2823–2834.

Piette, A., Fraipont, C., Den Blaauwen, T., Aarsman, M.E., Pastoret, S., and Nguyen-Distèche, M. (2004) Structural determinants required to target penicillin-binding protein 3 to the septum of *Escherichia coli*. *J Bacteriol* **186:** 6110–6117.

Pinho, M.G., and Errington, J. (2005) Recruitment of penicillin-binding protein PBP2 to the division site of *Staphylococcus aureus* is dependent on its transpeptidation substrates. *Mol Microbiol* **55:** 799–807.

Rafelski, S.M., and Theriot, J.A. (2006) Mechanism of polarization of *Listeria monocytogenes* surface protein ActA. *Mol Microbiol* **59:** 1262–1279.

von Rechenberg, M., Ursinus, A., and Höltje, J.V. (1996) Affinity chromatography as a means to study multienzyme complexes involved in murein synthesis. *Microb Drug Resist* **2:** 155–157.

Romeis, T., and Höltje, J.V. (1994) Specific interaction of penicillin-binding proteins 3 and 7/8 with soluble lytic transglycosylase in *Escherichia coli*. *J Biol Chem* **269:** 21603–21607.

Rothfield, L. (2003) New insights into the developmental history of the bacterial cell division site. *J Bacteriol* **185:** 1125–1127.

Simon, R., Priefer, U., and Pühler, A. (1983) A broad host range mobilization system for *in vivo* genetic engineering: transposon mutagenesis in gram negative bacteria. *Nat Biotechnol* **1:** 784–791.

Spratt, B.G. (1977) Temperature-sensitive cell division mutants of *Escherichia coli* with thermolabile penicillin-binding proteins. *J Bacteriol* **131:** 293–305.

Taschner, P.E., Ypenburg, N., Spratt, B.G., and Woldringh, C.L. (1988) An amino acid substitution in penicillin-binding protein 3 creates pointed polar caps in *Escherichia coli*. *J Bacteriol* **170:** 4828–4837.

Thanbichler, M., and Shapiro, L. (2006) MipZ, a spatial regulator coordinating chromosome segregation with cell division in *Caulobacter*. *Cell* **126:** 147–162.

Tiyanont, K., Doan, T., Lazarus, M.B., Fang, X., Rudner, D.Z., and Walker, S. (2006) Imaging peptidoglycan biosynthesis in *Bacillus subtilis* with fluorescent antibiotics. *Proc Natl Acad Sci USA* **103:** 11033–11038.

Vollmer, W., von Rechenberg, M., and Höltje, J.V. (1999) Demonstration of molecular interactions between the murein polymerase PBP1B, the lytic transglycosylase MltA, and the scaffolding protein MipA of *Escherichia coli*. *J Biol Chem* **274:** 6726–6734.

Vollmer, W., Blanot, D., and de Pedro, M.A. (2008) Peptidoglycan structure and architecture. *FEMS Microbiol Rev* **32:** 149–167.

Wang, L., Khattar, M.K., Donachie, W.D., and Lutkenhaus, J. (1998) FtsI and FtsW are localized to the septum in *Escherichia coli*. *J Bacteriol* **180:** 2810–2816.

Wang, Y., Jones, B.D., and Brun, Y.V. (2001) A set of *ftsZ* mutants blocked at different stages of cell division in *Caulobacter*. *Mol Microbiol* **40:** 347–360.

Weiss, D.S., Pogliano, K., Carson, M., Guzman, L.M., Fraipont, C., Nguyen-Distèche, M., *et al.* (1997) Localization of the *Escherichia coli* cell division protein FtsI (PBP3) to the division site and cell pole. *Mol Microbiol* **25:** 671–681.

Weiss, D.S., Chen, J.C., Ghigo, J.M., Boyd, D., and Beckwith, J. (1999) Localization of FtsI (PBP3) to the septal ring requires its membrane anchor, the Z ring, FtsA, FtsQ, and FtsL. *J Bacteriol* **181:** 508–520.

West, L., Yang, D., and Stephens, C. (2002) Use of the *Caulobacter crescentus* genome sequence to develop a method for systematic genetic mapping. *J Bacteriol* **184:** 2155–2166.

Wheeler, R.T., and Shapiro, L. (1999) Differential localization of two histidine kinases controlling bacterial cell differentiation. *Mol Cell* **4:** 683–694.

Wissel, M.C., and Weiss, D.S. (2004) Genetic analysis of the cell division protein FtsI (PBP3): amino acid substitutions that impair septal localization of FtsI and recruitment of FtsN. *J Bacteriol* **186:** 490–502.

Wissel, M.C., Wendt, J.L., Mitchell, C.J., and Weiss, D.S. (2005) The transmembrane helix of the *Escherichia coli*

© 2008 The Authors
Journal compilation © 2008 Blackwell Publishing Ltd,

division protein FtsI localizes to the septal ring. *J Bacteriol* **187:** 320–328.

Woldringh, C.L., Huls, P.G., Pas, E., Brakenhoff, G.J., and Nanninga, N. (1987) Topography of peptidoglycan synthesis during elongation and polar cap formation in a cell division mutant of *Escherichia coli* MC4100. *J Gen Microbiol* **133:** 575–586.

Yanouri, A., Daniel, R.A., Errington, J., and Buchanan, C.E. (1993) Cloning and sequencing of the cell division gene *pbpB*, which encodes penicillin-binding protein 2B in *Bacillus subtilis*. *J Bacteriol* **175:** 7604–7616.

Supporting information

Additional supporting information may be found in the online version of this article.

Please note: Wiley-Blackwell are not responsible for the content or functionality of any supporting materials supplied by the authors. Any queries (other than missing material) should be directed to the corresponding author for the article.

© 2008 The Authors
Journal compilation © 2008 Blackwell Publishing Ltd,